J. Min. Metall. Sect. B-Metall. 61 (2) (2025) 199 - 212

Journal of Mining and Metallurgy, Section B: Metallurgy

ENHANCING CORROSION RESISTANCE AND STRUCTURAL PROPERTIES OF Ni-TiO_2 COMPOSITE COATINGS: THE IMPACT OF SDS SURFACTANT

N. Ouhabab, E.G. Temam *, H.B. Temam, A. Gana, M. Althamthami

Physics Laboratory of Thin Films and Applications (PLTFA), University of Biskra, Biskra, Algeria

(Received 16 February 2025; Accepted 25 August 2025)

Abstract

Ni-TiO_2 composite coatings are promising materials for enhancing the corrosion resistance and structural properties of steel substrates in various industrial applications. Corrosion remains a major issue for steel components, prompting the need for effective protective coatings. This study investigates the influence of sodium dodecyl sulfate (SDS) surfactant on the structural, electrochemical, mechanical, and morphological properties of Ni-TiO_2 composite coatings electrodeposited on BS2 steel. The coatings were characterized using X-ray diffraction (XRD), scanning electron microscopy (SEM), energy-dispersive X-ray spectroscopy (EDX), microhardness testing, and electrochemical techniques, including potentiodynamic polarization and electrochemical impedance spectroscopy (EIS). The results show that SDS incorporation led to an increase in the crystallite size of the coatings, from 35.92 nm to 80.82 nm, and a significant enhancement in the relative texture coefficient (RTC) along the (200) plane (88.09%). SEM analysis revealed a more compact and uniform surface morphology, with SDS reducing surface porosity from 8.23×10^{-3}% to 2.20×10^{-6}%. Electrochemical measurements demonstrated a substantial improvement in corrosion resistance, with charge transfer resistance (R_{ct}) increasing from 5.17 k$\Omega\times cm^2$ to 312.65 k$\Omega\times cm^2$ and polarization resistance (R_p) rising from 2.5 k$\Omega\times cm^2$ to 176.38 k$\Omega\times cm^2$. The microhardness of the coatings decreased slightly from 256.26 kgf$\times mm^{-2}$ to 217.22 kgf$\times mm^{-2}$, indicating a trade-off between mechanical properties and enhanced corrosion protection. These findings highlight the potential of SDS as a valuable additive for optimizing Ni-TiO_2 composite coatings, although further research is needed to explore the impact of SDS concentration, long-term durability, and the performance of these coatings in more aggressive environments.

Keywords: *Ni-TiO_2; SDS; Corrosion resistance; Relative texture coefficient; Porosity reduction*

1. Introduction

Iron alloys, such as low carbon, mild, and stainless steel, are widely used in several industrial sectors. Iron alloys achieve high mechanical properties but have corrosion resistance [1–4]. Depositing a coating of a more corrosion resistant metal onto the iron alloy can improve its corrosion resistance. The electrodeposition of alloy and composite coatings improves the corrosion resistance of iron alloys. The electrodeposition technique is a versatile and effective method that offers a range of benefits and is widely employed in various industries to protect and enhance the performance of iron-based alloys [5].

The choice of metals for electrodeposition is vital for ensuring the corrosion resistance of coatings. Zinc, nickel, chromium, and cobalt are commonly used due to their excellent protective properties [6–8]. Nickel-based coatings, in particular, are widely used in corrosion protection. Zn-Ni alloy coatings, especially those with 1.5 wt.% Ni, have demonstrated superior corrosion resistance due to their stable γ-phase and basal texture in the Zn matrix [6]. Ni-Cr coatings, which benefit from the formation of continuous nickel hydroxide and compact chromium oxide passive films, demonstrate enhanced corrosion resistance with increased chromium content [7]. Ni-Co coatings, especially those with 10 wt.% Co, provide optimal corrosion resistance, attributed to improved electrochemical properties and a pronounced (111) orientation [8]. Composite coatings, such as Ni-Co-CNT and Ni-TiO_2, have also shown enhanced wear and corrosion resistance due to the incorporation of nanoparticles [9, 10].

Ni-TiO_2 composite coatings have been extensively studied for their enhanced corrosion resistance. The inclusion of TiO_2 particles in the Ni matrix significantly improves corrosion protection by shifting the corrosion potential towards more positive values, reducing corrosion current density, and increasing polarization resistance [11, 12]. The TiO_2 particles act as a physical barrier, preventing corrosive agents from reaching the metal surface, and this barrier effect is further enhanced by their uniform

Corresponding author: elhachemi.guettaf@univ-biskra.dz

https://doi.org/10.2298/JMMB2502160160

distribution within the Ni matrix, which is crucial for effective protection [11]. Moreover, the presence of TiO_2 particles leads to the formation of corrosion microcells that inhibit localized corrosion [13]. Increasing the TiO_2 content improves the material's corrosion resistance, while smaller TiO_2 particles contribute to better mechanical properties and more uniform distribution within the matrix, further enhancing both corrosion and mechanical performance [12, 14].

The addition of sodium dodecyl sulfate (SDS) surfactant to Ni-TiO_2 composite coatings offers several key advantages. SDS plays a crucial role in reducing particle agglomeration, thereby ensuring a more uniform distribution of nanoparticles within the coating matrix, which results in smoother and more consistent surfaces [15, 16]. This improved dispersion enhances the coating's surface properties, contributing to better mechanical strength and flexibility. The incorporation of SDS also significantly enhances corrosion resistance by creating a denser and more uniform coating that acts as an effective barrier against corrosive elements, with some coatings achieving protection efficiencies up to 87.9% [17]. Moreover, SDS contributes to the finer crystallization and improved microstructure of the coating, which is essential for high-performance applications [15]. Thus, the addition of SDS not only improves the surface and mechanical properties but also boosts the corrosion resistance of the composite coatings.

This study focuses on the synthesis of Ni-TiO_2 composite coatings using the electrodeposition technique, with the incorporation of sodium dodecyl sulfate (SDS) surfactant. The impact of SDS on the structural, surface morphology, coating porosity, and electrochemical properties of the coatings was systematically investigated in a 3.5% NaCl solution. Potentiodynamic polarization and electrochemical impedance spectroscopy (EIS) were employed to evaluate the corrosion resistance of the coatings. The results reveal that the addition of SDS significantly enhances corrosion resistance by reducing porosity and improving the relative texture coefficient (RTC). Electrochemical measurements demonstrated notable improvements in both polarization resistance (R_p), which increased to 176.38 $k\Omega \times cm^2$, and charge transfer resistance (R_{ct}), which rose to 312.645 $k\Omega \times cm^2$. These enhancements underline the potential of Ni-TiO_2-SDS composite coatings as highly effective anticorrosive materials for demanding applications, offering superior durability and protection in corrosive environments.

2. Materials and methods

The BS2 mild steel substrates (18 mm × 6.3 mm × 2.4 mm) were coated with electrodeposited Ni-TiO_2 composite coatings. The elemental composition of BS2 mild steel is 0.15% C, 0.75% Mn, 0.02% Si, 0.015% S, 0.012% P, 0.043% Al and Fe in equilibrium. The BS2 steel samples were polished with 120-1200 grit sandpaper, rinsed with distilled water, and dried with an air dryer. The clean substrates were placed in acetone solution to avoid further interaction with the surrounding medium. Before electrodeposition, the substrates were cleaned in an electrolyte solution containing 10 $g \times l^{-1}$ NaOH and 30 $g \times l^{-1}$ Na_2CO_3 to remove oil and grease. This process was conducted for 3 minutes at a current density of 2 $A \times dm^{-2}$. Then, the substrates were immersed in 10% HCl for 10 s to remove traces of oxides.

The chemical composition of the electrolytic bath is $NiCl_2 \times 6H_2O$ (23.7728 $g \times l^{-1}$), NH_4Cl (21.405 $g \times l^{-1}$), H_3BO_3 (18.5435 $g \times l^{-1}$), NaCl (5.8517 $g \times l^{-1}$), 10 $g \times l^{-1}$ of high purity (99%) TiO_2 powder (BIOCHEM Chemopharma, 315 Place Youville-Suite 343, Montreal, Quebec H2Y OA4, Canada; product code: 320150500) and SDS (5 $mmol \times l^{-1}$). Two sheets of pure nickel (99.9%) were partially immersed in the electrolyte to act as double sacrificed anodes. The composite coatings were electrodeposited for 1 hour at a current density of 3 $A \times dm^{-2}$, a pH of 4 and a temperature of 45 °C.

The coated BS2 steel substrates were subjected to XRD analysis with a scan step of 0.03° on an X-ray diffraction apparatus (Rigaku MiniFlex600) using a monochromatic ray CuKα (λ = 1.54056 Å) in the range of 10-100°. The surface morphology of the coated BS2 substrates was characterised using SEM analysis (TESCAN VEGA3). The elemental composition of the coatings was analysed using energy dispersive X-ray (EDX). Microhardness (HV) was measured using a Vickers microhardness tester (Wolpert Wilson Instruments model 402UD) at a load of 100 g and a dwell time of 10 s. HV measurement for the Ni-TiO_2 composite coating is not possible due to its complex surface morphology, including roughness, irregularities, and porosity, which prevent clear indentations. Karbasian et al. [18] noted that surface roughness distorts the indentation process, leading to inconsistent results. Pores and voids cause uneven indentation, and the heterogeneous grain structure leads to varying mechanical properties, as stated by Samal et al. [19] and Qu et al. [20]. Even cross-sectional measurements are compromised by these irregularities, as the coating's thickness and quality vary. Therefore, traditional microhardness testing is unsuitable.

Potentiodynamic polarization and EIS measurements were performed in an electrochemical workstation (GAMRY INSTRUMENTS, Ref: 3000-34109) consisting of a graphite anti-electrode, an Ag/AgCl reference electrode (saturated with KCl) and

the coatings as working electrodes. The electrochemical studies were conducted at room temperature in a 3.5 wt. % NaCl solution with a scan rate of 1 mV×s^{-1}. Before the measurements, all the samples were immersed in a 3.5 wt. % NaCl solution for 30 minutes to reach a steady state. The open circuit potential (OCP) and the EIS were measured in a frequency range from 0.01 Hz to 100 kHz.

3. Results and discussion

Figure 1 presents the X-ray diffraction (XRD) patterns of the BS2 steel substrate, TiO_2 powder, pure Ni coating, Ni-TiO_2 composite coating, and Ni-TiO_2-SDS composite coating, providing insights into the structural characteristics of each material. The BS2 steel XRD pattern (Figure 1a) reveals characteristic peaks at 44.64°, 64.85°, and 82.41°, corresponding to the (110), (200), and (211) planes of the α-Fe phase, confirming the crystallite structure of BS2 steel. The identified phases in the BS2 steel are ferrite and pearlite, typical of a ferrite-pearlite microstructure. These data serve as a baseline for evaluating the coatings applied to the steel substrate. The TiO2 powder XRD pattern (Figure 1b) shows both anatase

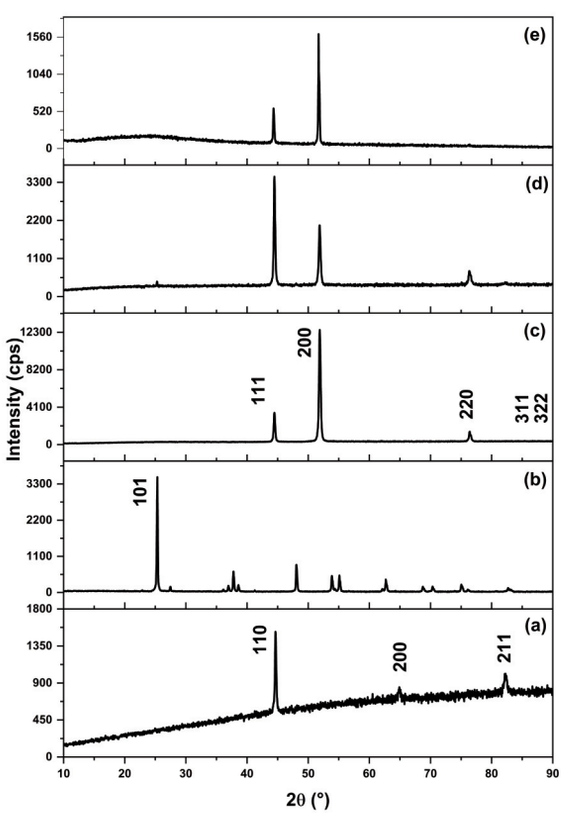

Figure 1. *XRD patterns: (a) BS2 steel substrate, (b) TiO_2 powder, (c) pure Ni coating, (d) Ni-TiO_2 composite coating, and (e) Ni-TiO_2+SDS composite coating*

Table 1. *RTC (%) and crystallite size of the coatings for the revealed planes*

Sample	(hkl)	Pure Ni	Ni-TiO_2	Ni-TiO_2-SDS
RTC (%)	(111)	7.76	25.59	11.91
	(200)	71.46	22.53	88.09
	(220)	12.42	17.07	–
	(311)	3.7	15.25	–
	(222)	4.66	19.56	–
Crystallite size (nm)	(111)	31.94	35.92	41.06
	(200)	29.59	36.97	80.82
	(220)	55.53	56.4	–
	(311)	22.63	48.25	–
	(222)	33.38	66.76	–

(ICDD 00-002-0387) and rutile phases (ICDD 00-002-0494), with a sharp peak at 2θ = 25.30° (101) confirming the presence of anatase. This combination of phases is known to enhance both mechanical properties and corrosion resistance in composite coatings [21].

The pure Ni coating (Figure 1c) exhibits a strong diffraction peak at 51.847° corresponding to the (200) plane (ICDD 00-004-0850), suggesting preferential growth along the (200) plane and high crystallinity, which contributes to the coating's mechanical strength and corrosion resistance. The Ni-TiO_2 composite coating (Figure 1d) shows Ni peaks with broadening, indicating that TiO_2 particles act as nucleation sites, influencing the crystallization of Ni and resulting in a finer-grained structure. The absence of distinct TiO_2 peaks reflects the fine dispersion of TiO_2 within the Ni matrix, a typical characteristic of composite coatings. Finally, the Ni-TiO_2-SDS composite coating (Figure 1e) demonstrates sharper, more intense diffraction peaks, indicating improved crystallinity. The presence of Sodium Dodecyl Sulfate (SDS) likely prevents TiO_2 agglomeration and enhances the uniformity of the crystallite structure. The clearer peaks, particularly along the (200) plane, suggest that SDS promotes crystallization in this direction. The absence of TiO_2 peaks further confirms the well-dispersed TiO_2 within the Ni matrix, contributing to the coating's structural integrity without forming a separate crystallite phase [13].

The Relative Texture Coefficient (RTC) is calculated to quantify the crystallographic orientation and texture of the coating, which is important for understanding its mechanical and corrosion-resistant properties. The RTC is determined using the following equation [22]:

$$RTC_{(hkl)} = \frac{I_{(hkl)} / I^0_{(hkl)}}{\sum_1^5 I_{(hkl)} / I^0_{(hkl)}} \times 100\% \quad (1)$$

where $I_{(hkl)}$ and $I^0_{(hkl)}$ are the diffraction intensities

of the (hkl) plane for the deposit and the standard Ni powder sample with reference code ICDD 00-004-0850, respectively. The five diffraction intensities along the (111), (200), (220), (311) and (222) planes are considered. The RTC values are summarized in Table 1. The pure Ni coating exhibits a high RTC of 71.46%, indicating dominant crystallite growth along the (200) plane, which enhances its mechanical strength and corrosion resistance. In the Ni-TiO_2 composite coating, the RTC drops to 25.59%, reflecting a shift in crystallite growth to the (111) plane, likely due to TiO_2 particles acting as nucleation sites. The Ni-TiO_2-SDS composite coating shows a significant increase in RTC to 88.09%, indicating improved crystallinity and preferred growth along the (200) plane. This suggests that Sodium Dodecyl Sulfate (SDS) enhances the uniformity and crystallinity of the coating, improving its mechanical and corrosion-resistant properties [16].

The crystallite size (D) is essential for understanding the mechanical strength and overall performance of the materials. The crystallite size is calculated using the following equation [23, 24]:

$$D = \frac{k\lambda}{\beta cos\theta} \quad (2)$$

Where k is a constant (0.89), λ is the wavelength of the X-ray radiation (λCukα=1.54056 Å), β is the full width at half maximum (FWHM) of the diffraction line, and θ is the diffraction angle. The calculated values of the crystallite size are summarized in Table 1.

The Ni-TiO_2-SDS composite coating shows the largest crystallite size of 80.82 nm, compared to pure Ni (29.59 nm) and Ni-TiO_2 (35.92 nm) coatings. This increase in crystallite size suggests that the addition of Sodium Dodecyl Sulfate (SDS) promotes the growth of larger Ni crystallites. F. Dogan et al. [25] found that surfactants like SDS enhance the crystallinity of coatings by preventing particle agglomeration. The larger crystallite size in the Ni-TiO_2-SDS composite coating indicates improved crystallinity, which is expected to enhance both its mechanical properties and corrosion resistance [26].

Figure 2 illustrates the effect of the surfactant sodium dodecyl sulfate (SDS) on the elemental composition of the Ni-TiO_2 composite coating, as analyzed through Energy Dispersive X-ray Spectroscopy (EDX). Figure 2a shows the successful co-deposition of TiO_2 particles in the Ni matrix, confirming the uniform distribution of TiO_2 within the coating. The presence of TiO_2 particles is evident in the elemental analysis, supporting the composite nature of the coating. Figure 2b results reveal a reduction in the Ti and O content when the coating is deposited using an SDS-containing solution. This decrease can be attributed to the excess SDS molecules, which coat both the TiO_2 particles and the cathode during deposition. This coating action prevents TiO_2 particles from fully contributing to the deposition process, ultimately reducing their content in the final coating. The reduction in the deposition rate due to SDS coverage is consistent with findings from previous studies, which suggest that SDS surfactant interferes with the particle deposition dynamics, influencing the overall coating composition [17].

Figure 3 presents the surface morphology of the coatings observed via scanning electron microscopy (SEM). Figure 3a shows the TiO_2 powder, with uniformly dispersed nanoparticles of varying sizes. Figure 3b depicts the pure Ni coating, exhibiting a smooth surface with nodular and pyramidal grains. Figure 3c reveals the Ni-TiO_2 composite coating, which has a rough, heterogeneous surface with cavities or gaps between protrusions, likely due to hydrogen evolution during co-deposition. Figure 3d shows the Ni-TiO_2-SDS composite coating, featuring uniform, pyramid-shaped protuberances. SDS improves grain uniformity, reduces voids, and levels the surface, enhancing the coating's mechanical and corrosion-resistant properties.

The particle size distribution of the nanoparticles was determined from SEM images and particle size histograms, as shown in Figure 4. Figure 4a reveals that the average particle size of the purchased TiO_2 powder is 324 nm. Figure 4b shows that the average particle size of the pure Ni coating is 212 nm.

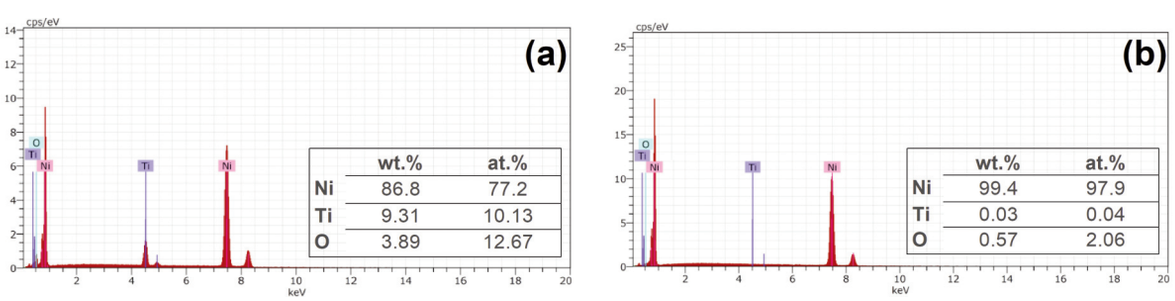

Figure 2. *EDX analysis of: (a) Ni-TiO_2 composite coating and (b) Ni-TiO_2-SDS composite coating*

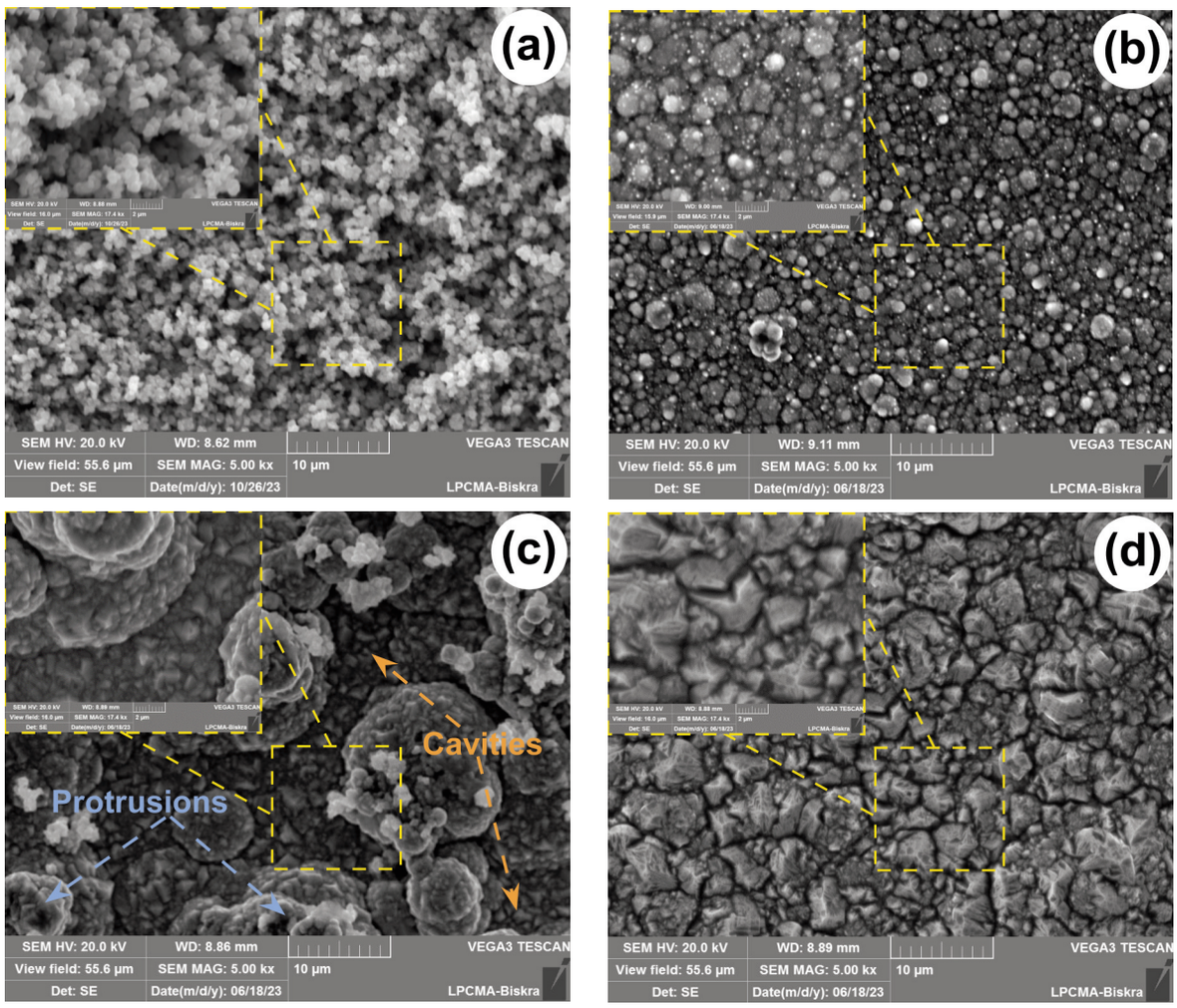

Figure 3. *SEM images of (a) TiO_2 powder, (b) pure Ni coating, (c) Ni-TiO_2, and (d) Ni-TiO_2-SDS composite coatings*

Incorporating TiO_2 nanoparticles into the Ni matrix (Figure 4c) increases the particle size to 336 nm due to the high concentration of TiO_2 (10 $g \times l^{-1}$), which causes nanoparticle agglomeration [27]. The addition of SDS surfactant (Figure 4d) reduces the particle size to 260 nm in the Ni-TiO_2 composite coating, likely due to the lower TiO_2 content. SDS also lowers the zeta potential of the TiO_2 particles, making them more negatively charged [28, 29].

Microhardness is often better understood in terms of dislocation density rather than crystallite size. Dislocations are linear defects in a material's atomic structure that are thermodynamically unstable. The dislocation density (ρ) represents the number of dislocations within a given area and was calculated using the following equation [23]:

$$\rho = \frac{1}{D^2} \tag{3}$$

When materials are subjected to stress, the atomic structure can distort, causing dislocations to form as the material tries to accommodate the stress. TiO_2 particles in the composite material can obstruct the movement of these dislocations, acting as physical barriers. Additionally, TiO_2 can serve as sites for dislocation storage, which leads to the formation of dislocation rings around the particles. The lattice strain (ε), which measures the distortion of the atomic lattice due to dislocations, can be calculated using the following equation [30]:

$$\varepsilon = \frac{\beta cos\theta}{4} \tag{4}$$

Table 2 summarizes the computed values for dislocation density (ρ), lattice strain (ε), and microhardness. It is evident that the values of ρ, ε, and microhardness decrease with the incorporation of TiO_2 particles and the addition of SDS surfactant. For

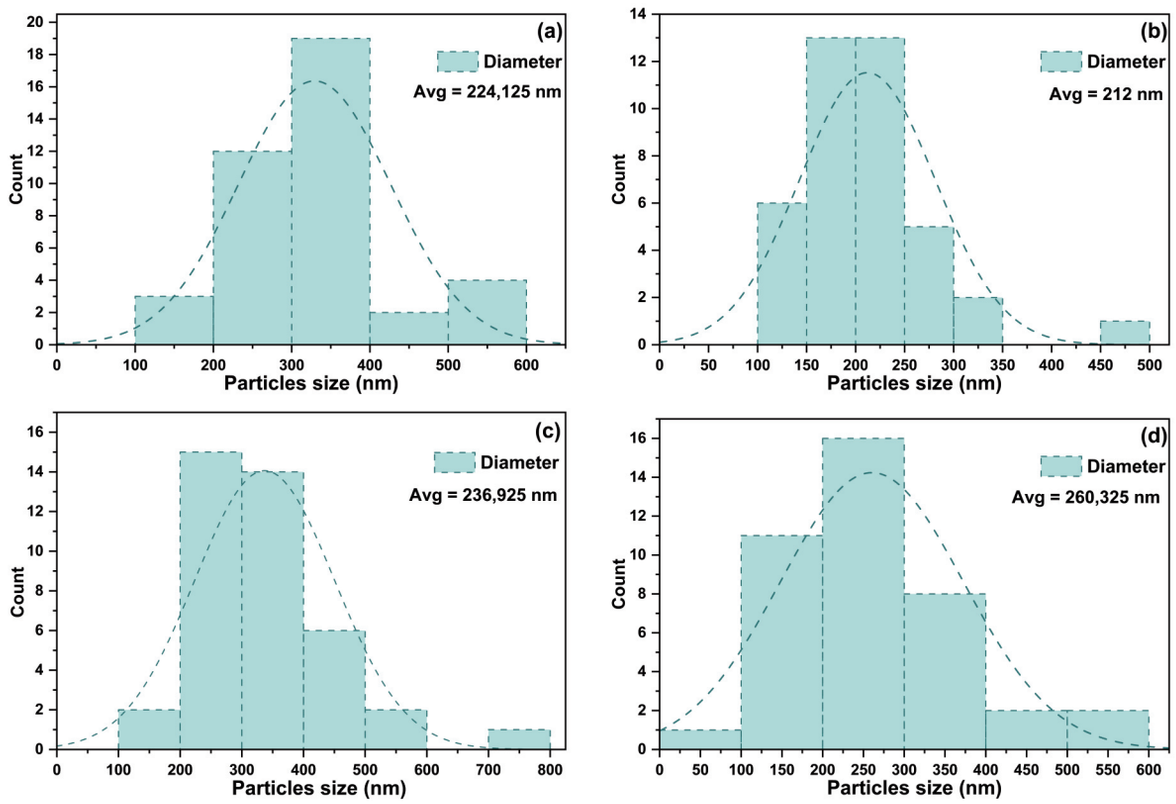

Figure 4. *Particles size distribution histogram determined from SEM image of (a) TiO_2 powder, (b) pure Ni coating, (c) Ni-TiO_2, and (d) Ni-TiO_2-SDS composite coatings*

instance, the dislocation density (ρ) decreases from 11.42×10^{-14} (lines×m^{-2}) in pure Ni to 7.32×10^{-14} (lines×m^{-2}) in the Ni-TiO_2 composite and further drops to 1.53×10^{-14} (lines×m^{-2}) in the Ni-TiO_2-SDS composite for the (200) plane. Similarly, the lattice strain (ε) decreases from 12×10^{-4} in pure Ni to 9.30×10^{-4} in Ni-TiO_2 and 4.24×10^{-4} in Ni-TiO_2-SDS for the (200) plane. The microhardness also shows a marked decrease, from 320.0 kgf×mm^{-2} in Ni-TiO_2 to 146.34 kgf×mm^{-2} in Ni-TiO_2-SDS for the (200) plane. This suggests that the TiO_2 particles and SDS surfactant introduce structural changes in the coating, resulting in increased dislocation storage and internal stress within the Ni matrix, which, in turn, reduces the material's overall hardness [31].

Table 2. *The calculated dislocation density, strain and microhardness*

Sample	(hkl)	Pure Ni	Ni-TiO_2	Ni-TiO_2-SDS
ρ×10^{-14} (lines×m^{-2})	(111)	9.8	7.75	5.93
	(200)	11.42	7.32	1.53
	(220)	3.24	3.14	–
	(311)	19.53	0.4.30	–
	(222)	9	2.24	–
ε×10^{-4} (%)	(111)	11	9.54	8.35
	(200)	12	9.3	4.24
	(220)	6	6.1	–
	(311)	15	7.1	–
	(222)	10	5.14	–
Microhardness (HV = 0.25 σ_y) (kgf×mm^{-2})	(111)	–	329.3	288.1
	(200)	–	320	146.34
	(220)	–	209.7	–
	(311)	–	245.1	–
	(222)	–	177.2	–

Table 3. *Average values of the dislocation density, strain, calculated and measured HV*

Sample	BS2	Pure Ni	Ni-TiO_2	Ni-TiO_2-SDS
ρ×10^{-14} (lines×m^{-2})	–	10.598	4.95	3.73
ε×10^{-4} (%)	–	10.8	7.436	6.295
HV = 0.25 σ_y (kgf×mm^{-2})	–	–	256.26	217.22
Avg HV (kgf×mm^{-2})	145	373.47	–	227.47

The microhardness of coatings is influenced by three mechanisms: grain refinement, particle strengthening, and dispersion strengthening [32–34]. Grain refinement increases hardness by hindering dislocation motion, as smaller grains increase

boundary areas. Particle strengthening occurs when particles like TiO_2 trap dislocations, while dispersion strengthening (Orowan mechanism) distributes dislocations around particles. The pure Ni coating shows 373.47 kgf×mm^{-2} hardness, while the Ni-TiO_2 composite coating (Figure 2b) complicates hardness measurement due to surface irregularities. Theoretical calculations give an average microhardness of 256.26 kgf×mm^{-2} (Table 3), determined using the following formula:

$$HV = 0.25\sigma_y \quad (5)$$

where HV is the Vickers microhardness (kgf×mm^{-2}) and σ_y is the yield stress in MN×m^{-2}. For hardening by dispersion, the yield stress is determined by the shear stress needed to bend a dislocation line between two particles separated by a distance of L_p, which is comparable to D. The maximum stress required for this, assuming the radius of curvature R = L_p/2, is given by the following equation:

$$\tau = \frac{G_b}{R} = \frac{2G_b}{L_p} \quad (6)$$

where G is the elastic shear modulus, and b is the Burgers vector. For Ni, G = 95 GPa and b = 0.249 nm [35, 36]. This method provides an estimate of the microhardness of the coating based on the dislocation densities.

Table 3 summarizes the measured and calculated microhardness (HV) values. The addition of Sodium Dodecyl Sulfate (SDS) surfactant influenced the Ni-TiO_2 composite coating's microstructure, changing it from nodular to pyramidal grains. This modification eliminated voids and elevations, leveled the surface, and suppressed undesirable secondary reactions. The dispersion strengthening mechanism, implemented through the Orowan mechanism, simplified the calculation process. The Ni-TiO_2-SDS composite coating shows a microhardness of 256.26 kgf×mm^{-2} (Table 3), which is lower than that of the pure Ni coating (373.47 kgf×mm^{-2}) and the Ni-TiO_2 composite coating (320.0 kgf×mm^{-2}). Despite this, all coatings have improved microhardness compared to the bare BS2 steel, which has a microhardness of 145 kgf×mm^{-2} (Table 3).

The potentiodynamic polarization curves were recorded from -400 mV to 400 mV relative to the open circuit potentials (OCPs), with a scan rate of 1 mV×s^{-1}. The exposed area of the working electrode to the electrolyte solution is 2.85 cm^2. Figure 5 shows the OCPs and polarization curves. Each sample was immersed in a corrosion cell containing 300 ml of a 3.5 wt. % NaCl solution for 1 hour at room temperature. The OCP curves are shown in Figure 5a, while the corresponding polarization plots are presented in Figure 5b. Electrochemical parameters, including corrosion potential (E_{corr}), corrosion current density (I_{corr}), corrosion rate (r_{corr}), and anodic and cathodic Tafel slopes (β_a and β_c) were determined using linear polarization theory. Calculating the polarization resistance is essential as it provides a quantitative measure of the coating's ability to resist corrosion. The polarization resistance (R_p) was determined using the Stern-Geary Equation (Eq.7) [37]:

$$R_p = \frac{\beta_a \beta_c}{i_{corr}\left(\beta_a + \beta_c\right) ln10} \quad (7)$$

where β_a and β_c are the anodic and cathodic Tafel slopes, respectively, which describe the rate of the electrochemical reactions at the electrode surface. icorr is the corrosion current determined from the polarization curves using the Tafel fit method. The fitted parameter values are summarized in Table 4.

The results show that the addition of SDS to the electrodeposition bath significantly enhances the corrosion resistance of the resulting Ni-TiO_2 composite coating. The SDS-modified coating exhibited a corrosion potential (E_{corr}) of -143.0 mV, compared to -340.0 mV for the Ni-TiO_2 coating, indicating improved corrosion resistance. The lower E_{corr} suggests that the SDS surfactant forms a protective barrier, reducing the coating's susceptibility to corrosion. The corrosion current density (I_{corr}) for the SDS-modified coating was 0.141 µA×cm^{-2}, much lower than 1.382 µA×cm^{-2} for the Ni-TiO_2 coating. This decrease indicates a reduced corrosion rate, as the surfactant limits the electrochemical reactions at the coating surface. Similarly, the corrosion rate (r_{corr}) for the SDS-modified coating dropped to 1.694 µmpy, compared to 16.62 µmpy for the Ni-TiO_2 coating, further confirming the enhanced protection. These improvements in E_{corr}, I_{corr}, and r_{corr} suggest that SDS enhances the corrosion resistance by forming a protective barrier that prevents the diffusion of corrosive ions to the coating surface, reducing the overall corrosion rate [3, 38].

For the Electrochemical Impedance Spectroscopy (EIS) measurements, the samples were immersed in a 3.5 wt. % NaCl solution for 30 minutes at room temperature to stabilize the coating-electrolyte interface. The EIS studies were conducted within the frequency range of 0.01-100 Hz. Figure 6 illustrates the OCPs, Bode and Nyquist plots, along with the corresponding equivalent electrical circuit models for BS2 bare and coated substrates.

As shown in Figure 6a, the higher Open Circuit Potential (OCP) values correlate with more corrosion-

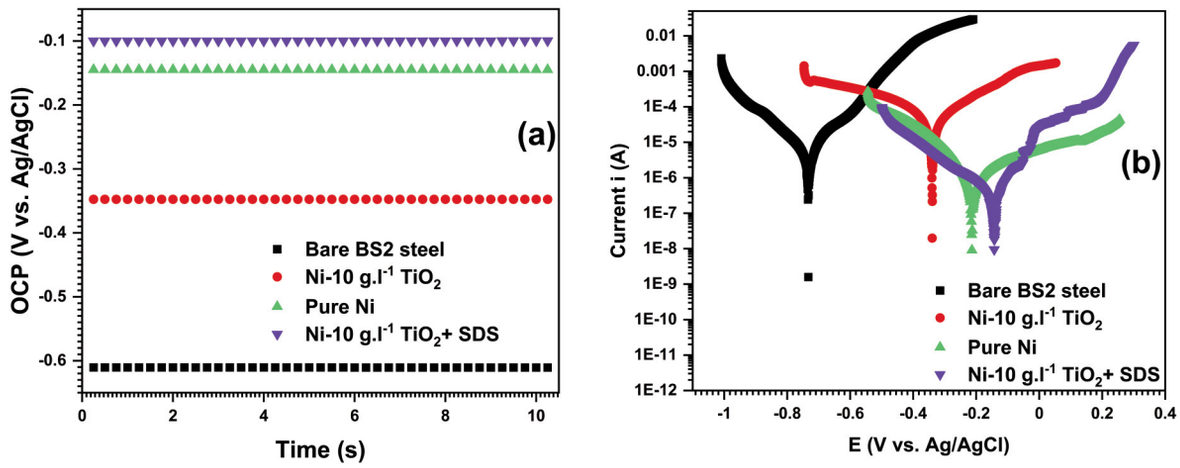

Figure 5. *(a) OCPs and (b) potentiodynamic polarization curves of the samples*

Table 4. *Fitted parameters extracted from the polarization curves*

Sample	BS2	Pure Ni	Ni-TiO_2	Ni-TiO_2-SDS
OCP (mV)	-610.636	-144.816	-347.629	-99.4639
E_{corr} (mV)	-733	-214	-340	-143
I_{corr} (μA×cm^{-2})	1.853	0.41	1.382	0.141
r_{corr} (μmpy)	35.78	4.933	16.62	1.694
β_a (mV/dec)	110	253	432.9	84.4
β_c (mV/dec)	123.9	105.7	294.5	178.1
R_p (kΩ×cm^2)	13.657	78.97	2.5006	176.38

resistant materials, suggesting that coatings enhance the overall electrochemical stability. Figure 6b presents the Bode impedance modulus spectra, revealing a marked improvement in corrosion resistance for the coated substrates, particularly indicated by an increase in impedance modulus at lower frequencies (from around 0.04 Hz to 0.01 Hz). The Bode phase spectra in Figure 6c exhibit peaks at approximately (2 Hz, -66°) for the BS2 steel and (3.2 Hz, -69°) for the Ni-TiO_2 composite coating. The pure Ni coating shows two additional broad peaks spanning from 0.8 Hz to 63 Hz, while the Ni-TiO_2-SDS composite coating has two broad peaks ranging from 0.5 Hz to 38.4 Hz. This suggests two distinct temporal parameters: the low-frequency peak likely reflects the coating's interface with the BS2 steel, while the high-frequency peak relates to the outermost layer of the coating [39].

The Nyquist plots in Figure 6d are modelled by the equivalent circuits shown in Figure 6e. The larger diameters of the quasi-semicircles for the pure Ni coating (157.434 kΩ×cm^2) and the Ni-TiO_2-SDS composite coating (312.645 kΩ×cm^2) indicate significantly higher corrosion resistance compared to the bare BS2 steel (1.5912 kΩ×cm^2) and the Ni-TiO_2 composite coating (5.1699 kΩ×cm^2). The enhanced corrosion resistance of the Ni-TiO_2-SDS composite coating can be attributed to the anionic effect of SDS, which prevents chloride (Cl^-) ions from reaching the substrate via electrostatic interactions and reduces the formation of hydrogen bubbles on the cathodic surface, thereby minimizing pitting and porosity [17].

The equivalent circuit model for the bare BS2 steel and the Ni-TiO_2 coating (shown in Figure 6e1) consists of two capacitive loops, one at high frequency and an inductive loop at low frequency. This configuration can be explained by the accumulation of corrosion products at the steel surface and at the coating-substrate interface [40]. The model includes solution resistance (Rs), a constant phase element (CPE) representing the double-layer capacitance, charge transfer resistance (R_{ct}), inductance (L), and resistance (RL). On the other hand, the equivalent circuit for the pure Ni coating and Ni-TiO_2-SDS composite coating (shown in Figure 6e2) comprises two capacitive loops: one associated with the morphological characteristics of the coating, and the other linked to electron transfer and the charge-discharge processes of the electrical double layer between the electrode surface and the electrolyte [41].

The fitted parameters for these models, as summarized in Table 5, reveal that the double-layer capacitance (Y_{dl}) decreases from 461.40 μS×cm^{-2} (for

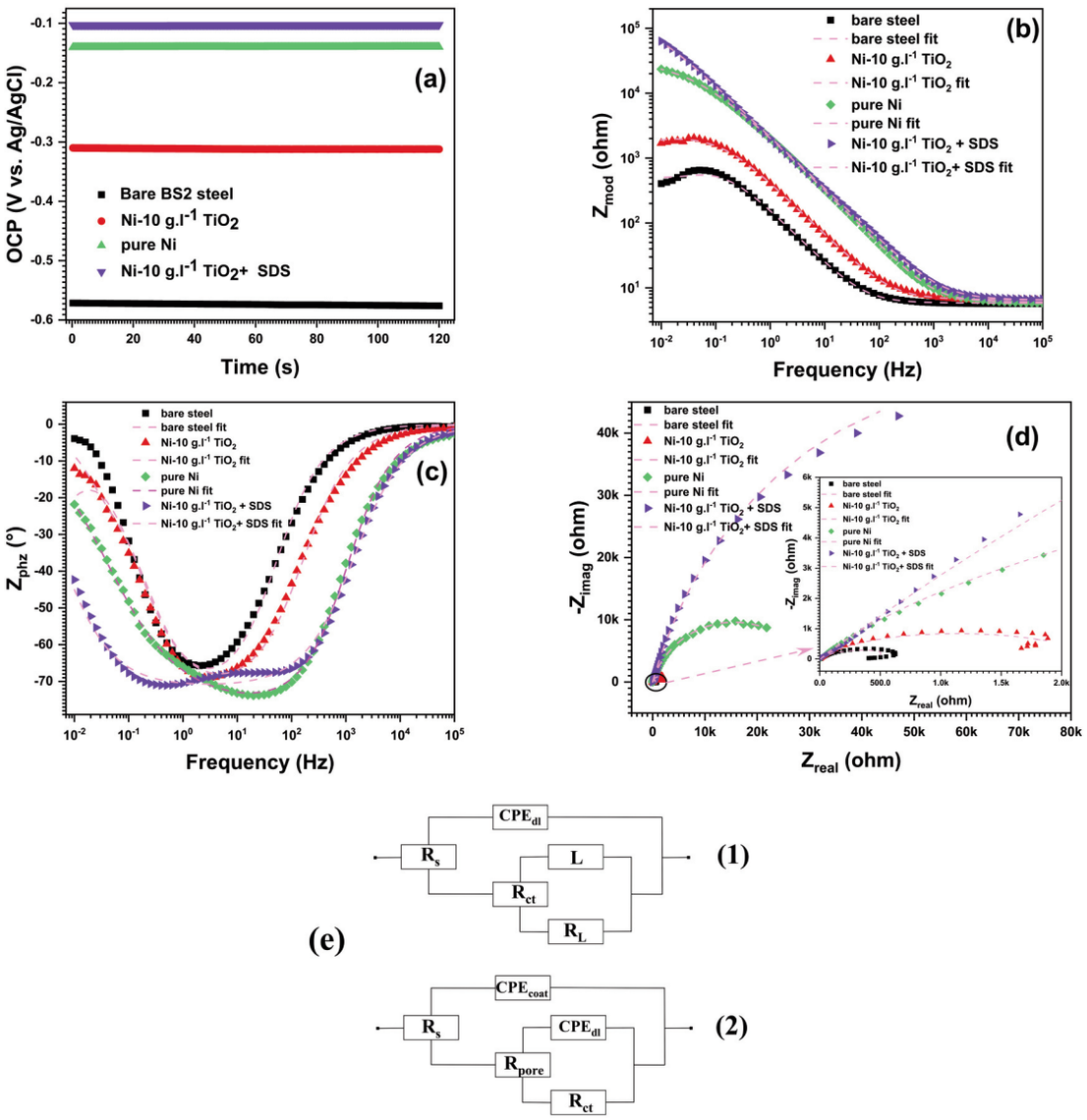

Figure 6. *EIS potentiostatic plots: (a) OCPs, (b) Bode impedance modulus spectra, (c) Bode phase spectra and (d) Nyquist spectra (e) Equivalent electrical circuit models for: (1) bare BS2 steel substrate and Ni-TiO_2 coating and (2) pure Ni coating and Ni-TiO_2-SDS composite coating*

Table 5. *Parameter values of equivalent electrical circuit models used for fitted EIS measurements*

Sample	BS2	Pure Ni	Ni-TiO_2	Ni-TiO_2-SDS
Rs (Ω)	5.81	6.514	6.572	6.655
Y_{dl} (μS×s^{ndl}×cm^{-2})	461.4	14.288	180.95	10.323
n_{dl}	0.8412	0.7647	0.8176	0.8186
R_{ct} (kΩ×cm^2)	1.5912	157.434	5.1699	312.645
L (kH×cm^2)	-1.4073	–	-10.574	–
RL (kΩ×cm^2)	0.61389	–	1.93	–
Y_{coat} (μS×S^{ncoat}×cm^{-2})	–	20.323	–	28.628
n_{coat}	–	0.8402	–	0.8308
R_{pore} (kΩ×cm^2)	–	5.8311	–	4.0328
Goodness of fit	8.239×10^{-3}	178.9×10^{-6}	1.579×10^{-3}	70.08×10^{-6}

the pure Ni coating) to 10.323 μS×S^{ndl}×cm^{-2} (for the Ni-TiO_2-SDS composite coating), reflecting the enhanced barrier properties of the latter. Furthermore, the coating resistance (R_{pore}) and the Y_{coat} values provide additional insights into the corrosion protection performance of the coatings. The impedance of the CPE (ZCPE) is defined as follows:

$$Z_{CPE} = \frac{1}{Y_0 (j\omega)^n} \quad (8)$$

Where Y_0, j = √-1, ω and n are the admittance constant, imaginary unit, angular frequency and dimensionless empirical exponent, respectively. The parameter n corresponds to the phase angle deviation and characterises the heterogeneity of the electrode surface. High values of n are typical of a smooth substrate, and those close to unity indicate a prominent capacitive advantage [42, 43].

Porosity in the coatings was evaluated using both polarization (Eq.9) and EIS (Eq.10) data. The results indicate that the polarization resistance (R_p) values are consistent with the charge transfer resistance (R_{ct}) values, reinforcing the reliability of the porosity measurements derived from both techniques. The porosity percentage can be calculated using the following equations [44]:

$$P_{R_p} = \left(\frac{R_{p\,bare}}{R_{p\,coating}} \right) \times 10^{-\left(\frac{\Delta E_{corr}}{\beta_a} \right)} \times 100 \quad (9)$$

$$P_{R_p} = \left(\frac{R_{p\,bare}}{R_{p\,coating}} \right) \times 10^{-\left(\frac{\Delta E_{corr}}{\beta_a} \right)} \times 100 \quad (10)$$

where P_{Rp} and P_{Rct} represent the porosity (%) calculated from polarization and EIS measurements, respectively. ΔE_{corr} is the difference in the corrosion potentials from the polarization curve. R_{Pbare} and $R_{Pcoating}$ are the polarization resistances of the bare BS2 steel and coated sample, respectively. Table 6 summarizes the porosity values, and Figure 7 shows that lower porosity correlates with better corrosion resistance. Notably, the the addition of SDS to the electrodeposition bath leads to a substantial reduction in porosity, from 8.23×10^{-3}% in the Ni-TiO_2 coating to just 2.20×10^{-6}% in the Ni-TiO_2-SDS coating. In comparison, the pure Ni coating exhibits a porosity of 3.31×10^{-4}%, further emphasizing the effectiveness of SDS in enhancing the coating's compactness. This decrease in porosity is attributed to the formation of densely packed pyramid-shaped protuberances on the coating surface, a direct result of the SDS surfactant's suppressive effect on the hydrogen evolution reaction during deposition [16, 45].

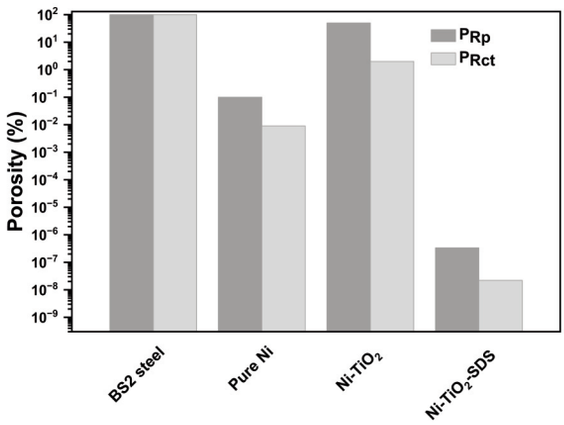

Figure 7. *Porosity values calculated from the polarization curves (P_{Rp}) and EIS data (P_{Rct})*

Table 6. *Porosity values calculated from polarization resistance (P_{Rp}) and electrochemical impedance spectroscopy (P_{Rct}) for different coatings*

Sample	BS2	Pure Ni	Ni-TiO_2	Ni-TiO_2-SDS
P_{Rp} (%)	100	3.31x10^{-4}	1.46x10^{-1}	3.35x10^{-5}
PR_{ct} (%)	100	1.93×10^{-5}	8.23x10^{-3}	2.20x10^{-6}

These findings highlight the crucial role of SDS in improving both the structural and electrochemical properties of Ni-TiO_2 composite coatings. By reducing porosity and enhancing corrosion resistance, SDS significantly boosts the protective performance of the coatings, making them more suitable for demanding industrial applications. However, a slight reduction in microhardness suggests a trade-off between mechanical strength and corrosion resistance, indicating that further optimization is necessary to enhance the overall performance without compromising strength.

4. Conclusion

In this study, the addition of SDS significantly enhanced the structural, electrochemical, and mechanical properties of Ni-TiO_2 composite coatings. SDS enhanced the crystallinity of the Ni-TiO_2 coatings, which increased from 35.92 nm to 80.82 nm, and the relative texture coefficient (RTC) along the (200) plane was enhanced to 88.09%. X-ray diffraction (XRD) analysis revealed that the incorporation of TiO_2 particles into the Ni matrix resulted in a shift in crystallite growth towards the (111) plane. The surface morphology, observed through scanning electron microscopy (SEM), demonstrated a significant improvement in coating uniformity and compactness, with SDS reducing surface porosity from 8.23×10^{-3}% to 2.20×10^{-6}%. The more uniform surface morphology, along with the reduction in porosity, contribute to the formation of a

more protective and durable coating. These structural and morphological enhancements are key factors in the improved corrosion resistance observed in the coatings. However, the microhardness of the coatings decreased slightly, from 256.26 kgf×mm^{-2} to 217.22 kgf×mm^{-2}. This reduction in hardness can be attributed to the increased crystallite size and the possible formation of a less dense microstructure due to the SDS surfactant. The surfactant's role in enhancing particle dispersion may also contribute to the observed decrease in hardness. The increase in the crystallite size leads to a reduction in dislocation density, which typically influences the material's hardness. The findings suggest that these SDS-modified coatings are particularly promising for applications requiring enhanced corrosion resistance, such as in marine, automotive, and industrial environments where steel components are exposed to aggressive conditions. These coatings offer a balance of improved durability and ease of application, but further optimization is necessary to enhance mechanical properties without compromising corrosion protection. Future work should focus on exploring the long-term performance of these coatings under real-world conditions and investigating the impact of varying SDS concentrations to fine-tune the balance between corrosion resistance and mechanical strength.

Acknowledgements

The authors would like to thank the Algerian Directorate General for Scientific Research and Technological Development-DGRSDT for financial assistance.

Author's contribution

N. Ouhabab: Investigation, Methodology, Data curation, Writing – original draft. E.G. Temam: Conceptualization, Supervision, Review & Editing, Project administration, Funding acquisition. H. B. Temam: Validation, Formal analysis, Visualization, Resources. A. Gana: Data curation, Formal analysis, Writing – review & editing. M. Althamthami: Review, Editing, Project coordination.

Data availability

Data will be made available on request.

Conflict of interest

The authors declare that they have no known competing financial interests or personal relationships that could have appeared to influence the work reported in this paper.

References

[1] H. Liu, C. Feng, Z. Wang, Y. Zhang, D. Zhang, Y. Yan, Study of fretting-initiated crevice corrosion and crevice corrosion affected fretting of stainless steel, Corrosion Science, 225 (2023) 111586. https://doi.org/10.1016/J.CORSCI.2023.111586

[2] Y. Sun, W. Liu, L. Chen, T. Zhang, H. Li, B. Zhang, W. Yang, J. Cui, B. Hou, F. Wang, B. Dong, The dual nature of Cu content on the corrosion resistance of low alloy steels in sulfuric acid: A time-dependent reversal of corrosion resistance, Corrosion Science, 224 (2023) 111486. https://doi.org/10.1016/J.CORSCI.2023.111486

[3] H. Cheng, H. Luo, X. Wang, X. Li, Microstructure and corrosion resistance properties of (FeCoNi)86Al7Ti7 high-entropy alloy via different aging time, Corrosion Science, 226 (2024) 111670. https://doi.org/10.1016/J.CORSCI.2023.111670

[4] L. Chen, W. Liu, H. Li, Y. Sun, B. Zhang, Z. Sun, Interaction between silty sand and temperature towards corrosion behavior of carbon steel in CO_2 environment, Corrosion Science, 224 (2023) 111522. https://doi.org/10.1016/J.CORSCI.2023.111522

[5] Z. Zou, M. Xu, L. Ma, T. Xue, B. Wang, Corrosion resistance of multistep doped graphene oxide/lanthanum-based/silane composite coatings on the magnesium alloys, Molecular Crystals and Liquid Crystals, 764 (1) (2023) 90-102. https://doi.org/10.1080/15421406.2023.2204562

[6] K.S. Jyotheender, M. Mathai, S.K. Makineni, C. Srivastava, Nickel partitioning in ZnNi coatings (Ni less than 4 wt.%) and its effect on the coating corrosion behaviour, Philosophical Magazine, 103 (18) (2023) 1701–1716. https://doi.org/10.1080/14786435.2023.2231355

[7] Y. Zhu, C.Q. Gu, J. Wang, X. Xi, Z. Qin, Characterization and corrosion behavior of Ni-Cr coatings by using pulse current electrodeposition, Anti-Corrosion Methods and Materials, 70 (5) (2023) 236–242. https://doi.org/10.1108/ACMM-04-2023-2788

[8] Y. Chen, H. Yang, H. Feng, P. Yang, J. Zhang, B. Shu, Electrodeposition and corrosion performance of Ni-Co alloys with different cobalt contents, Materials Today Communications, 35 (2023) 106058. https://doi.org/10.1016/J.MTCOMM.2023.106058

[9] S. Yang, Z. Zhang, K. Xu, Y. Wu, H. Zhu, W. Shen, Y. Liu, Investigation of the enhancement mechanism of electrochemically deposited Ni-Co-W coatings via laser irradiation: effect of W contents on corrosion resistance, Langmuir, 39 (29) (2023) 10079–10087. https://doi.org/10.1021/ACS.LANGMUIR.3C01020

[10] N. Ouhabab, E.G. Temam, H.B. Temam, A. Gana, Improvement of the microstructure and corrosion behavior of Ni-TiO_2 composite coatings electrodeposited at various amounts of TiO_2 powder, Studies in Engineering and Exact Sciences, 5 (2) (2024) e9185. https://doi.org/10.54021/seesv5n2-336

[11] Y. Wang, Z. Miao, S. Zheng, J. Chen, Z. He, An Investigation into electrodeposited Co−Ni−TiO_2 films with improved mechanical and corrosion properties, Coatings, 13 (4) (2023) 783. https://doi.org/10.3390/COATINGS13040783

[12] Y.A. Chien, C.Y. Chen, T. Kurioka, M. Sone, T.F.M. Chang, High strength Ni matrix TiO_2 composites by supercritical CO_2 assisted Co-electrodeposition with

different sizes of TiO_2 particle, Micro and Nano Engineering, 20 (2023) 100219. https://doi.org/10.1016/J.MNE.2023.100219

[13] P.G. John, M.E. Sahayaraj, J.W. Jappes, S.J. Leon, Corrosion characteristics of microwave and furnace annealed electroless Ni-P-TiO_2 coatings, Proceedings of the Institution of Mechanical Engineers, Part C: Journal of Mechanical Engineering Science, 238 (4) (2024) 1149–1156. https://doi.org/10.1177/09544062231179086

[14] P.S. Raju, A.V.N.L. Sharma, A. Gopichand, Inexpensive production of hydrophobic and corrosion resistant titania-silica composite coatings for deep water sandwich pipe applications, Australian Journal of Mechanical Engineering, 23 (1) (2025) 51–56. https://doi.org/10.1080/14484846.2023.2231599

[15] H. Rao, W. Li, F. Zhao, Y. Song, H. Liu, L. Zhu, H. Chen, Electrodeposition of high-quality Ni/SiC composite coatings by using binary non-ionic surfactants, Molecules, 28 (8) (2023) 3344. https://doi.org/10.3390/molecules28083344

[16] M. Zhu, Z. Zhu, X. Xu, C. Xu, Surfactant improved interface morphology and mass transfer for electrochemical oxygen-evolving reaction, Catalysts, 13 (3) (2023) 569. https://doi.org/10.3390/catal13030569

[17] L. Guerguer, A. Hamdi, A. Ziouche, D. Benbertal, M.A. Belalem, A. Benmoussat, Influence of surfactant concentration on structural properties and corrosion behaviour of electrodeposited Ni-SiO_2 nanocomposite coatings, International Journal of Materials Research, 114 (3) (2023) 175–190. https://doi.org/10.1515/ijmr-2021-8429

[18] A. Karbasian, M. Shirazi, A.H. Mahmoudi, Effect of surface roughness on brinell hardness and load-displacement curves using a macro indentation, International Journal of Engineering, 36 (5) (2023) 914–924. https://doi.org/10.5829/ije.2023.36.05b.08

[19] S. Samal, J. Zeman, J. Kopeček, P. Šittner, The microstructure, hardness, phase transformation and mechanical properties of a NiTi coating applied to graphite substrate via a plasma spraying process, Coatings, 13 (7) (2023) 1174. https://doi.org/10.3390/coatings13071174/S1

[20] S. Qu, K. Zheng, J. Gao, Y. Ma, J. Zhi, S. Yu, S. Xie, Y. Xin, B. Zhou, Y. Wang, Diamond particles-reinforced Ni-based composite coating on Ti6Al4V alloy: Microstructure, mechanical, dynamic impact and dry-sliding tribological properties, Surface and Coatings Technology, 458 (2023) 129307. https://doi.org/10.1016/J.SURFCOAT.2023.129307

[21] K. Simfroso, S.R. Cabo, R. Unabia, A. Britos, P. Sokołowski, R. Candidato, Solution precursor plasma spraying of TiO_2 coatings using a catalyst-free precursor, Materials, 16 (4) (2023) 1515. https://doi.org/10.3390/MA16041515

[22] B. Do Lee, J.W. Lee, J. Ahn, S. Kim, W.B. Park, K.S. Sohn, A deep learning approach to powder x-ray diffraction pattern analysis: Addressing generalizability and perturbation issues simultaneously, Advanced Intelligent Systems, 5 (9) (2023) 2300140. https://doi.org/10.1002/aisy.202300140

[23] E.U. Morales-Cruz, M. Vargas-Ramírez, A. Lobo-Guerrero, A. Cruz-Ramírez, E. Colin-García, R.G. Sánchez-Alvarado, V.H. Gutiérrez-Pérez, J.M. Martínez-Vázquez, Effect of low aluminum additions in the microstructure and mechanical properties of hot forged high-manganese steels, Journal of Mining and Metallurgy, Section B: Metallurgy, 59 (1) (2023) 77–90. https://doi.org/10.2298/JMMB220919007M

[24] B.T. Hachemi, M. Zarour, O. Bacha, E.G. Temam, A. Mekkaoui, Corrosion inhibition effect of arabic gum on Cu-WC nanocomposite coating synthesized by electrodeposition technology, Journal of Applied Engineering Science & Technology, 5 (1) (2025) 108. https://doi.org/10.69717/JAEST.V5.I1.108

[25] F. Doğan, E. Duru, M. Uysal, H. Akbulut, S. Aslan, Structural, mechanical, and tribological studies of Ni-B-TiN composite coating: effect of SDS concentration, Journal of Adhesion Science and Technology, 37 (6) (2023) 1010–1033. https://doi.org/10.1080/01694243.2022.2060784

[26] H. Dhiflaoui, S. Ben Salem, M. Salah, Y. Dabaki, S. Chayoukhi, B. Gassoumi, A. Hajjaji, A. Ben Cheikh Larbi, M. Amlouk, H. Benhayoune, Influence of TiO_2 on the microstructure, mechanical properties and corrosion resistance of hydroxyapatite HaP + TiO_2 nanocomposites deposited using spray pyrolysis, Coatings, 13 (7) (2023) 1283. https://doi.org/10.3390/COATINGS13071283

[27] Y.A. Chien, C.Y. Chen, T. Kurioka, M. Sone, T.F.M. Chang, High strength Ni matrix TiO_2 composites by supercritical CO_2 assisted Co-electrodeposition with different sizes of TiO_2 particle, Micro and Nano Engineering, 20 (2023) 100219. https://doi.org/10.1016/j.mne.2023.100219

[28] L. Liccardo, M. Bordin, P.M. Sheverdyaeva, M. Belli, P. Moras, A. Vomiero, E. Moretti, Surface defect engineering in colored TiO_2 hollow spheres toward efficient photocatalysis, Advanced Functional Materials, 33 (22) (2023) 2212486. https://doi.org/10.1002/adfm.202212486

[29] M. Machreki, T. Chouki, G. Tyuliev, D. Žigon, B. Ohtani, A. Loukanov, P. Stefanov, S. Emin, Defective TiO_2 nanotube arrays for efficient photoelectrochemcal degradation of organic pollutants, ACS Omega, 8 (24) (2023) 21605–21617. https://doi.org/10.1021/acsomega.3c00820

[30] H. Xie, Z. Yang, Q.S. Ma, W. Meng, L. Hu, X.H. Yin, Effect of extrusion process on the stress corrosion cracking resistance of 7N01 aluminum alloy, Journal of Mining and Metallurgy, Section B: Metallurgy, 59 (1) (2023) 137–146. https://doi.org/10.2298/jmmb221229012x

[31] H. Gül, The effect of TiO_2 concentration on morphology, wear and corrosion properties of NiB-TiO_2 composite coatings by ultrasonic-assisted pulse electrodeposition, Surface Topography: Metrology and Properties, 11 (1) (2023) 015001. https://doi.org/10.1088/2051-672x/acaff9

[32] A.A. Khan, A.K. Hossain, M.S. Kaiser, The role of Si at a lower level on the mechanical properties of Al-based automotive alloys, Journal of Mining and Metallurgy, Section B: Metallurgy, 59 (1) (2023) 147–154. https://doi.org/10.2298/jmmb230131013k

[33] P. Li, L. Li, L. Tang, L. Wang, J. Xu, L. Dong, X. Mao, Y. Liu, Y. Zhang, Micron-sized SiC particles reinforced TC_4 composites: Mechanical properties and strengthening mechanisms, Materials Today Communications, 38 (2024) 108147. https://doi.org/10.1016/j.mtcomm.2024.108147

[34] X. Mao, P. Zhu, X. Sun, S. Huang, C. Xu, H. He, Y.

Chen, Z. Cheng, Nucleation mechanism, particle shape and strengthening behavior of (Ti, Nb) (C, N) particles in Fe-based composite coatings by plasma spray welding, Ceramics International, 50 (15) (2024) 27296–27304. https://doi.org/10.1016/j.ceramint.2024.05.027

[35] P. Zhang, Y. Zhao, J. Huang, J. Li, L. Cao, J. Liu, G. Han, W. Du, L. Chen, L. Xiao, Q. Wang, Y. Yang, S. Zhu, W. Li, Enhanced mechanical and wear properties of Ni-W-SiC composite coatings by synergistic influence of micro-nano SiC mixture, Surface and Coatings Technology, 467 (2023) 129678. https://doi.org/10.1016/j.surfcoat.2023.129678

[36] M. Sun, C. Ding, J. Xu, D. Shan, B. Guo, T. G. Langdon, Microhardness and microstructural evolution of pure nickel processed by high-pressure torsion, Crystals, 13 (6) (2023) 887. https://doi.org/10.3390/cryst13060887

[37] D. Jullian, A. Prillieux, D.B. Hibbert, J. Zhang, D.J. Young, Internal oxidation of austenitic Fe-Ni-Cr alloys at high temperatures: Deduction of oxygen permeability and the influence of carbon-bearing gases, Corrosion Science, 224 (2023) 111465. https://doi.org/10.1016/j.corsci.2023.111465

[38] Z. Pan, H. Luo, Q. Zhao, H. Cheng, X. Li, Effect of Hf addition on microstructural evolution and corrosion behavior of nickel-based alloys in hydrochloric acid, Corrosion Science, 224 (2023) 111507. https://doi.org/10.1016/j.corsci.2023.111507

[39] M. Krbata, P. Fabo, M. Kohutiar, J. Escherova, M. Kuba, M. Kianicova, M. Eckert, Possibilities of using impedance spectroscopy for indirect measurements of thin layers of Al & Cr-Al coatings on Ni-based superalloy inconel 713LC applied by the "Out-of-pack" diffusion method, Manufacturing Technology, 23 (3) (2023) 313–318. https://doi.org/10.21062/mft.2023.042

[40] M. Wang, H. Sun, X. Zhou, P. Wang, Y. Zhang, X. Wang, X. Zhang, D. Hou, M. Wang, Atomistic insights into the deposition of corrosion products on the surfaces of steels and passivation films, Langmuir, 39 (19) (2023) 6812–6822. https://doi.org/10.1021/acs.langmuir.3c00363

[41] N.A. Ismail, R.A. Shakoor, R. Kahraman, Corrosion inhibition performance of developed epoxy coatings containing carbon nanocapsules loaded with diethylenetriamine, Progress in Organic Coatings, 183 (2023) 107716. https://doi.org/10.1016/j.porgcoat.2023.107716

[42] Y. Hou, T. Guo, M. Bance, C. Jiang, A high-precision circuit-simulator-compatible model for constant phase element using rational function approximation, IEEE Journal of the Electron Devices Society, 11 (2023) 726–733. https://doi.org/10.1109/jeds.2023.3292824

[43] M. Wilson L. Cowie, V. Farrow, M. Cree, J. Scott, Rapid time-domain simulation of fractional capacitors with SPICE, Journal of Computational Electronics, 23 (3) (2024) 677–689. https://doi.org/10.1007/s10825-024-02160-x

[44] I.M. Makena, M.B. Shongwe, Effects of porosity on the corrosion behaviour of PM-fabricated titanium foams for biomedical applications, International Journal of Electrochemical Science, 19 (3) (2024) 100495. https://doi.org/10.1016/j.ijoes.2024.100495

[45] Y. Liu, P. Yang, Y. Li, Y. Xiao, B. Shu, Effect of sodium dodecyl sulfate (SDS) on the co-deposition and frictional behavior of carbon nanotube/nickel composite layer, Materials Research Express, 11 (4) (2024) 046508. https://doi.org/10.1088/2053-1591/ad3ba2

POBOLJŠANJE OTPORNOSTI NA KOROZIJU I STRUKTURNIH SVOJSTAVA KOMPOZITNIH PREVLAKA Ni-TiO_2: UTICAJ SURFAKTANTA SDS

N. Ouhabab, E.G. Temam *, H.B. Temam, A. Gana, M. Altamtami

Laboratorija za fiziku tankih filmova i primene (PLTFA), Univerzitet u Biskri, Biskra, Alžir

Apstrakt

Kompozitne prevlake Ni-TiO_2 predstavljaju obećavajuće materijale za poboljšanje otpornosti na koroziju i strukturnih svojstava čeličnih podloga u različitim industrijskim primenama. Korozija ostaje značajan problem za čelične komponente, što nameće potrebu za efikasnim zaštitnim prevlakama. Ova studija ispituje uticaj surfaktanta natrijum-dodecil-sulfata (SDS) na strukturna, elektrohemijska, mehanička i morfološka svojstva kompozitnih prevlaka Ni-TiO_2 elektrodeponovanih na čeliku BS2. Prevlake su karakterisane primenom difrakcije X-zraka (XRD), skenirajuće elektronske mikroskopije (SEM), energetsko-disperzivne spektroskopije X-zraka (EDX), ispitivanja mikrotvrdoće i elektrohemijskih tehnika, uključujući potenciodinamičku polarizaciju i elektrohemijsku impedansnu spektroskopiju (EIS). Rezultati pokazuju da je inkorporacija SDS dovela do povećanja veličine kristalita prevlaka, sa 35,92 nm na 80,82 nm, i značajnog poboljšanja relativnog koeficijenta teksture (RTC) duž ravni (200) (88,09%). SEM analiza je otkrila kompaktniju i ujednačeniju morfologiju površine, pri čemu je SDS smanjio poroznost površine sa $8{,}23\times10^{-3}$% na $2{,}20\times10^{-6}$%. Elektrohemijska merenja su pokazala značajno poboljšanje otpornosti na koroziju, pri čemu se otpor prenosa naelektrisanja (R_{ct}) povećao sa 5,17 kΩ×cm^2 na 312,65 kΩ×cm^2, a polarizacioni otpor (R_p) porastao sa 2,5 kΩ×cm^2 na 176,38 kΩ×cm^2. Mikrotvrdoća prevlaka je blago opala sa 256,26 kgf×mm^{-2} na 217,22 kgf×mm^{-2}, što ukazuje na kompromis između mehaničkih osobina i poboljšane zaštite od korozije. Ovi nalazi ističu potencijal SDS kao vrednog aditiva za optimizaciju kompozitnih prevlaka Ni-TiO_2, iako su potrebna dalja istraživanja kako bi se ispitao uticaj koncentracije SDS, dugoročna izdržljivost i performanse ovih prevlaka u agresivnijim sredinama.

Ključne reči: *Ni-TiO_2; SDS; Otpornost na koroziju; Relativni koeficijent teksture; Smanjenje poroznosti*